ACCOUNTS of chemical research

Article

pubs.acs.org/accounts

Revising Intramolecular Photoinduced Electron Transfer (PET) from First-Principles

Daniel Escudero*,†

†CEISAM UMR CNRS 6230, Université de Nantes, 2 rue de la Houssinière, BP 92208, 44322 Cedex 3 Nantes, France

Supporting Information

CONSPECTUS: Photoinduced electron transfer (PET) plays relevant roles in many areas of chemistry, including charge separation processes in photovoltaics, natural and artificial photosynthesis, and photoluminescence sensors and switches. As in many other photochemical scenarios, the structural and energetic factors play relevant roles in determining the rates and efficiencies of PET and its competitive photodeactivation processes. Particularly, in the field of fluorescent sensors and switches, intramolecular PET is believed (in many cases without compelling experimental proof) to be responsible of the quench of fluorescence. There is an increasing experimental interest in fluorophore's molecular design and on achieving optimal excitation/emission spectra, excitation coefficients, and fluorescence quantum yields (importantly for bioimaging purposes), but less efforts are devoted to fundamental mechanistic studies. In this Account, I revise the origins of the fluorescence quenching in some of these systems with state-of-the-art quantum chemical tools. These studies go beyond the common strategy of analyzing frontier orbital energy diagrams and performing PET thermodynamics calculations. Instead, the potential energy surfaces (PESs) of the lowest-lying excited states are explored with time-dependent density functional theory (TD-DFT) and complete active space self-consistent field (CASSCF) calculations and the radiative and nonradiative decay rates from the involved excited states are computed from first-principles using a thermal vibration correlation function formalism. With such a strategy, this work reveals the real origins of the fluorescence quenching, herein entitled as dark-state quenching. Dark states (those that do not absorb or emit light) are often elusive to experiments and thus, computational investigations can provide novel insights into the actual photodeactivation mechanisms. The success of the dark-state quenching mechanism is demonstrated for a wide variety of fluorescent probes, including proton, cation and anion targets. Furthermore, this mechanism provides a general picture of the fluorescence quenching which englobes intramolecular charge-transfer (ICT), ratiometric quenching, and those radiationless mechanisms believed to be originated by PET. Finally, this Account provides for the first time a computational protocol to quantitatively estimate this phenomenon and provides the ingredients for the optimal design of fluorescent probes from first principles.

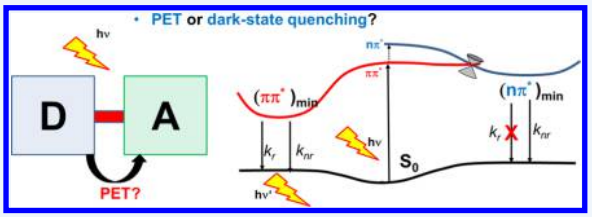

1. INTRODUCTION

Photoinduced electron transfer (PET) from a donor (D) to an acceptor (A) leads to the formation of a charge separated state consisting of the donor radical cation and the acceptor radical anion.[1,2] In an intramolecular PET process, D and A coexist in the same molecule, while in an intermolecular PET they correspond to different molecules. PET is of crucial importance in many chemical and biological scenarios, e.g., from photovoltaics[3] and photoluminescence sensors and switches[4,5] to natural[6] and artificial[7] photosynthesis. The kinetics and thermodynamics basis for the intermolecular PET process are known since the seminal works of Marcus[8,9] and Weller,[10] in the 1950s and 1960s, respectively. PET is modulated by the electrochemical and excited state properties of the acceptor and donor moieties. As in other photochemical playgrounds, intermolecular and/or intramolecular PET is in direct competition with many other radiative and nonradiative deactivation processes occurring in the excited states of molecular systems.[11] Overall, PET leads to a decrease of both lifetimes and emission quantum yields. However, it is often neglected that other mechanisms may be responsible of the fluorescence quenching, e.g., from internal conversion (IC) and intersystem crossing (ISC) mechanisms to energy transfer processes. To unambiguously prove the existence of PET and quantify its rate, the detection of radical ions with time-resolved spectroscopies is required. Hence, charge separation or recombination (back electron transfer) can be probed by for instance laser flash photolysis experiments, which measure the transient absorption of the radical anion and cation species.[12,13] Other techniques such as time-resolved resonance Raman, electron spin resonance and infrared spectroscopies can also provide information regarding charge separation and recombination.[14,15] Despite their tremendous interest, intramolecular PET processes have less exhaustively been studied with these techniques[13,16,17] as compared to intermolecular processes. Particularly, in the field of fluorescent sensors and switches, any observed fluorescence quenching is in many cases automatically ascribed to PET without compelling experimental proofs (see in Scheme 1 the generally accepted mechanism of an intramolecular PET-based

Received: June 16, 2016
Published: August 30, 2016

DOI: 10.1021/acs.accounts.6b00299
Acc. Chem. Res. 2016, 49, 1816−1824

Scheme 1. General Accepted Mechanism of an Intramolecular PET Fluorescent Probe (D−A)[a]

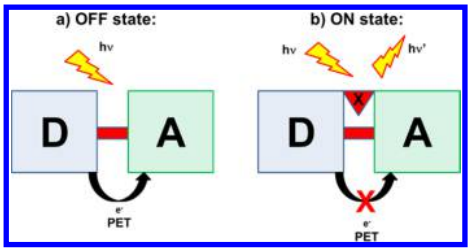

[a](a) PET in the the analyte-free D-A system creates the OFF state. (b) Addition of an analyte (X) blocks the PET mechanism and activates the fluorescence emission, resulting in the ON state.

fluorescent probe). Often, frontier molecular orbital calculations along with optical and electrochemical experiments on both ON and OFF states (see Scheme 1) are reported in these studies. In Scheme 2, the schematic frontier molecular orbital diagrams for

Scheme 2. Frontier Molecular Orbital Energy Diagrams of the OFF (a) and ON (b) States of an A−D System[a]

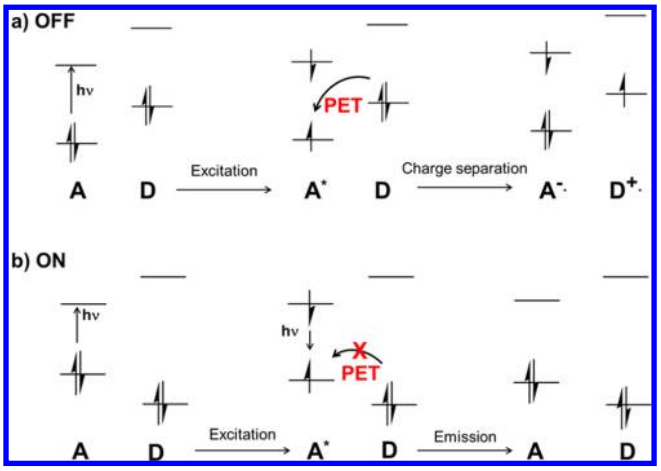

[a]In the OFF state (a), the HOMO level corresponds to the D-based orbital, so that PET is thermodynamically feasible. In the ON state (b), the HOMO level is the A-based orbital, so that PET is not plausible.

PET and its energetic requirements are shown. With these data at hand, the thermodynamic feasibility and the kinetic rates of the formation of the charge separated state can be estimated (i) via the Weller and Marcus expressions or (ii) in a qualitative fashion (e.g., comparing the orbital energies of the ON and OFF states; see Scheme 2). It is important to remark that even if a PET process is thermodynamically feasible, it does not imply its occurrence since it might not be fast enough to compete with other possible photodeactivation processes. Furthermore, geometrical and orbital relaxation effects are neglected when evaluating the frontier molecular orbitals only at the ground state geometries, and hence it may lead to erroneous predictions of a putative PET process. In this Account, I revise the origins of the quenching of fluorescence in some fluorescent probes, i.e., from proton targets to cation and anion targets, with quantum chemical tools. These studies go far beyond the common strategy of analyzing frontier molecular orbital diagrams. Instead, I characterize the PESs of the lowest-lying excited states (only a few mechanistic studies have been reported so far)[18,19] and I compute the radiative and nonradiative efficiencies from the involved excited states. In this regard, recent theoretical developments[20] have extended the applications from a qualitative assignment of the absorption and emission properties to a quantitative interpretation of both photochemical reactivity and photoluminescence properties.[21,22] With such a strategy, this work reveals the real origins of the quench of fluorescence in the studied fluorescent probes, herein entitled as dark-state quenching effect, and it provides for the first time a computational approach to quantitatively estimate the quenching effect. In photochemistry, dark excited states are those that do not absorb or emit light. Consequently, they are difficult to track with spectroscopic techniques. However, they are known to play pivotal roles in the radiationless deactivation of many molecular systems, including polyenes,[23] aromatic compounds[24] and carotenoids.[25] Furthermore, the dark-state quenching mechanism enables unifying all possible types of fluorescence quenching, from those believed to be originated by PET to intramolecular charge transfer (ICT). This Account is structured as follows: In section 2 is presented a general and cheap computational strategy (based on TD-DFT calculations) that permits the evaluation of the dark-state mechanism on a semiquantitative basis for large-size systems. In section 3, an amine−fluorophore system used as a proton target fluorescent probe, and for which detailed experimental spectroscopic data are available, is studied in detail. Furthermore, a computational strategy to quantify the quenching effect is presented for the latter compound.

2. THE DARK-STATE QUENCHING MECHANISM: TOWARD A GENERAL COMPUTATIONAL STRATEGY

Secondary and tertiary amines intramolecularly linked to fluorophore systems are the most widespread proton target fluorescent sensors.[26] Arsenical-[27] and phosphorus-based[28] dyes are also used with the same purposes. In this section I examine the fluorescence properties of several fluorescent probes, i.e. from proton (**1** in Scheme 3) targets to cation (**3**) and anion (**5**) targets. The final goal is to develop a general and cheap computational protocol that permits (i) the study of large organic fluorophores and (ii) the rationalization of the fluorescence quenching on a semiquantitative basis beyond frontier molecular orbital energy diagrams. In order to prove the existence of the dark-state quenching mechanism, the PESs of **1**−**6** were explored with TD-PBE0 calculations (see details in the Supporting Information (SI), a comparison with the experimental absorption and emission properties in Table S1 and the orbitals involved in the electronic excitations in Figures S1−S3). The imidazo[1,5-*a*]pyridinium derivative **1** exhibits a complete turn-on of fluorescence under acidic conditions.[29] The fluorescence properties of aromatic amines (i.e., anilines) have been widely studied both experimentally[30,31] and computationally,[32] especially those of 4-(dimethylamino)benzonitrile (DMABN) and aminobenzonitrile (ABN). For the latter compounds, exhaustive computational studies on their photodeactivation pathways are available.[33,34] The fluorescence properties of anilines are determined by a subtle competition between different photodeactivation pathways, involving both local excited (LE) and ICT (PICT) states.[35] Dual (or multi) fluorescence is often observed on these systems.[31] LE and planar ICT states (PICT) are mainly responsible of their emission characteristics while rehybridized ICT (RICT) states have been assigned both computationally and with transient absorption experiments.[36] Contrarily, the population of a twisted ICT (TICT) state, characterized by a torsional motion of the amino

DOI: 10.1021/acs.accounts.6b00299
Acc. Chem. Res. 2016, 49, 1816−1824

Scheme 3. Chemical Structure of Compounds 1−6

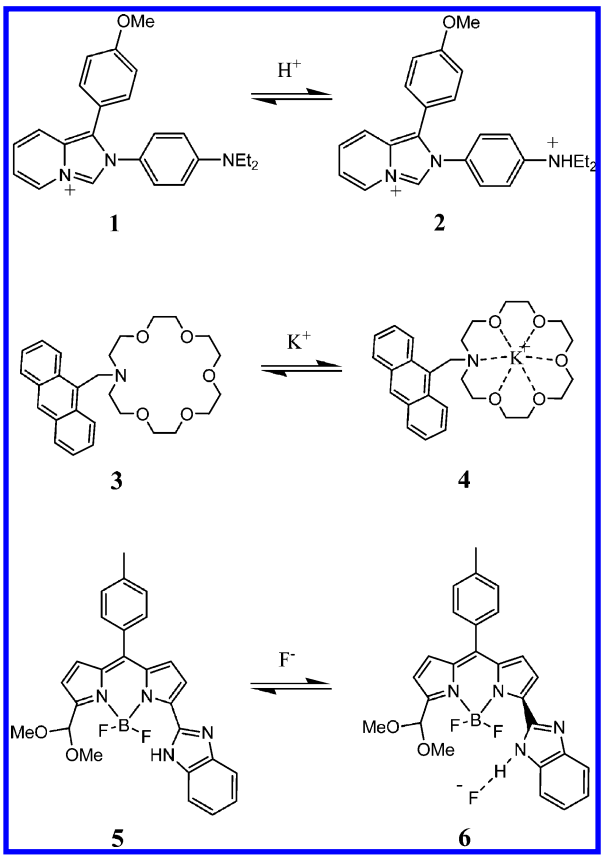

group with respect to the phenyl ring, considerably enhances the radiationless deactivation to the ground state,[35] although in recent reports these states have also been assigned as the emissive species under special conditions (i.e., for some DMABN derivatives in polar solvents).[36] Despite all the experimental and computational evidence, PET is still assigned as responsible of the fluorescence quenching in many aniline derivatives; see, for instance, in refs 37 and 38. Important geometrical relaxation effects occur along the photodeactivation pathways of these systems, and thus it further stresses the drawbacks of using a static approach consisting of examining the frontier molecular orbitals at the ground state optimized geometries. In Figure 1a and b, the potential energy profiles for **1** and **2** are schematically presented, respectively. Vertical absorption and emission energies, along with their oscillator strengths, are also included (see computational details in the SI). The spectroscopic state of **1** is S_1 (HOMO → LUMO transition, see the orbitals involved in Figure 1a). At the ground state geometry, the amino group is coplanar with the phenyl ring and the lone pair orbital of the amino group is delocalized within the phenyl ring at the HOMO orbital (see Figure 1a). Consequently, this electronic excitation is characterized by a notorious oscillator strength ($f = 0.115$). After the initial excitation to the S_1 state, the system evolves during its photodeactivation pathway along a torsional motion involving the amino group, which finally leads to the $(S_1)_{min}$ geometry. At this geometry, the amino group is twisted with respect to the phenyl group, and thus it corresponds to a TICT species. At the TICT minimum, the lone pair of the amino group is no longer delocalized within the phenyl ring, so that its oscillator strength becomes negligible ($f = 0.000$) and hence becomes a dark state. The important geometrical relaxation effects along with the negligible oscillator strength at the TICT minimum makes the radiationless deactivation to the ground state much preferred over the radiative deactivation. These computational evidence are in agreement with the nearly complete observed turn-off of fluorescence in **1** ($\Phi_{fluo} = 0.06\%$).[29] Contrarily, in the protonated species (**2**), relaxation on the S_1 PES leads to a LE minimum, characterized by a non-negligible oscillator strength ($f = 0.055$). Therefore, in **2**, the radiative depopulation to the ground state can now compete to radiationless decay. Indeed, a turn-on of fluorescence ($\Phi_{fluo} = 42\%$) is experimentally observed upon acidification.[29] The fluorescence quenching observed when going from **2** to **1** is thus, complete. Two main features may lead to a partial fluorescence quenching instead of a complete one: first in cases where the initial excited state population is branched between competing deactivation channels (see exemplarily for compound **7** in section 3) and second in cases where the character of the final state at its relaxed geometry has a non-negligible oscillator strength (such as, e.g., in the case that a mixed ICT/LE state is obtained). In the second case, oppositely to the first one, a shift in the emission energy usually accompanies the changes in the fluorescence properties. This partial quenching is generally found in ratiometric fluorescent probes.[29]

Let us move the discussion to the fluorescent probe for cations (**3**). Compound **3** also acts as a fluorescent probe for protons.[39] Experimentally, the fluorescence quantum yield increases from nearly zero in the metal-free system (**3**, $\Phi_{fluo} = 0.03\%$) to $\Phi_{fluo} =$ 14% upon addition in excess of a potassium salt (so that the formation of **4** is expected to be quantitative). The spectroscopic states of **3** are S_1 and S_2, which are both of mixed $\pi\pi^*$/ $n\pi^*$ character (see their vertical absorption energies and associated oscillator strengths in Figure 1c). Relaxation on the S_1 PES leads to $(n\pi^*)_{min}$ while relaxation on the S_2 PES leads to $(\pi\pi^*)_{min}$. Importantly, in **3**, the $\pi\pi^*$ state remains S_2 at its optimized geometry. Therefore, $S_2 \rightarrow S_1$ IC is likely to occur, and thus the well of the dark $n\pi^*$ state is always populated regardless of the photoexcitation energy according to the Kasha rule. The latter state is characterized by a very low oscillator strength ($f = 0.001$), thus explaining the complete quench of fluorescence in **3.** Contrarily, in **4**, due to potassium-amine electrostatic interaction, the $n\pi^*$ state is pushed upward in energy (see S_3 in Figure 1d), so that it is not populated on the course of photodeactivation. Therefore, the fluorescence properties of **4** are dominated by the fluorophore-like $\pi\pi^*$ photophysics.

Finally, to complete the discussion on different fluorescent probes, compound **5**, a fluorescent probe for anions, is discussed. The boron-dipyrromethene (BODIPY) derivative **5** is selective for F^-.[40] The fluorescence quenching is caused by the deprotonation of the benzimidazole moiety. Once deprotonated, it is believed that PET from the benzimidazole to the BODIPY unit is responsible for the turn-off of fluorescence. In Figure 1e and f, the excited state PES of **5** and **6** are schematically depicted. Indeed, at the optimized ground state geometry of **6**, a proton transfer from the benzimidazole to F^- atom takes place. Consequently, the character of the lowest excited states changes from **5** to **6**. Thus, the photophysical properties in **5** (which is the ON species) are dominated by the BODIPY $\pi\pi^*$-based photophysics. Oppositely, in **6**, the S_1 state becomes a dark state with ICT character from the benzimidazole to the BODIPY moiety (HOMO → LUMO transition in Figure 1f). Initial excitation to the bright S_2 state is followed by $S_2 \rightarrow S_1$ IC, which finally leads to the population of the well of the S_1. At the $(S_1)_{min}$ the benzimidazole unit is twisted with respect to the BODIPY core. The very important geometrical relaxations along this deactivation pathway in conjunction with the vanishing oscillator

DOI: 10.1021/acs.accounts.6b00299
Acc. Chem. Res. 2016, 49, 1816−1824

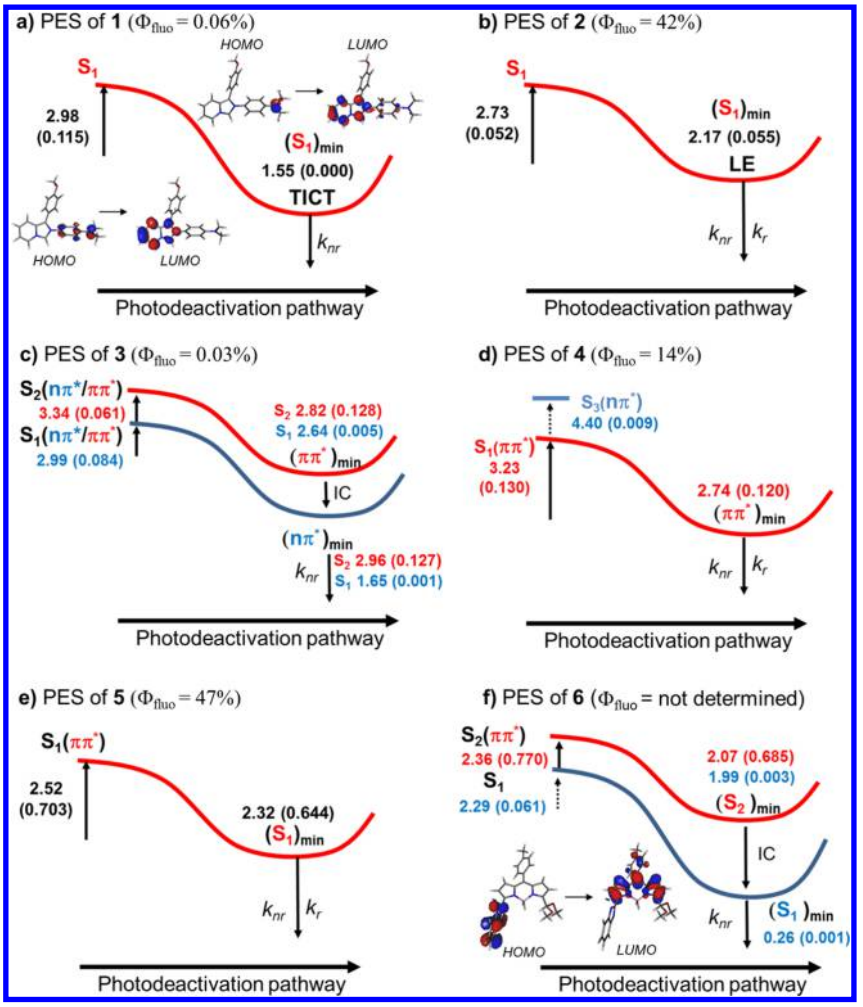

Figure 1. Schematic potential energy profiles (TD-PBE0/6-31G*) of compounds **1**−**6**. Energies are in eV, and oscillator strengths are given between parentheses. The experimental fluorescence quantum yields are also included.

strength (f = 0.000), point to a complete quench of fluorescence in **6**. Experimentally, the fluorescence intensity of **5** gradually decreases upon addition of F^- and it is completely quenched in the presence of 15 equiv of F^- (so that the quantitative formation of **6** is expected),[40] in agreement to the theoretical predictions. These findings are also in agreement to other fluorescent probes, including thiol[41] and BODIPY derivatives,[42] where dark states of ICT character are found to be responsible of the fluorescence quenching.

As demonstrated for compounds **1**−**6**, but also in other recent works,[43,44] the computational approach consisting of characterizing the PESs of the low-lying excited states with TD-DFT methods can already provide a semiquantitative estimation of the dark-state quenching effect occurring on a wide variety of fluorescent probes. Hence, upon photodeactivation, the final population of dark states of different character (e.g., ICT and nπ* states) is responsible for the fluorescence quenching. The excited state population is trapped in the well of the dark state, so that the radiationless deactivation to the ground state is very likely. As demonstrated in this Account, the dark-state quenching mechanism is operative for three different fluorescent probes and also for those systems reported in refs 40−44. In view of this evidence, this mechanism can presumably be extrapolated to other scenarios. Certainly, this mechanism might not always be operative for all possible fluorescent probes. In conflictive cases, to assess whether PET competes to nonradiative decay, further experimental support might be required. From a methodological point of view, TD-PBE0 succeds to provide an adiabatic description of the excited states of complexes **1**−**6**. However, nonadiabatic effects (those originated by the crossing between PESs) are often relevant in these systems.[19] In these cases, single-reference methods (such as TD-DFT) should be used carefully, especially in the vicinity of the crossing points. Hence, the obtainment of nonadiabatic photoinduced pathways mediated by conical intersections requires the use of multiconfigurational ab initio methods, such as the complete active space self-consistent field (CASSCF) method (see exemplarily the discussion for compound **7** in Section 3).

3. TOWARD A QUANTITATIVE ESTIMATION OF THE FLUORESCENCE QUENCHING: AN AMINOANTHRACENE DERIVATIVE AS A CASE STUDY

The aminoanthracene derivative (**7**) showed in Scheme 4 is a fluorescent probe for protons and it is reminiscent of **3**. Compound **7** has recently been studied with time-resolved spectroscopies under different pH conditions.[45] Upon acidification, the acid−base equilibrium is displaced toward the protonated species (**8**). The protonation of amine-fluorophore systems commonly leads to a fluorescence enhancement (of both quantum yields and lifetimes). Exemplarily, in **7**, the fluorescence

DOI: 10.1021/acs.accounts.6b00299
Acc. Chem. Res. 2016, 49, 1816−1824

Scheme 4. Chemical Structure of Compounds 7 and 8

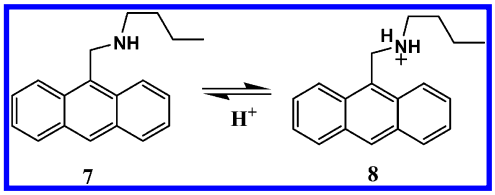

lifetime raises from 5.17 ns at neutral pH to 7.05 ns in acidic conditions (almost quantitative formation of **8** is expected at the latter conditions).[45] The partial quench of fluorescence in the unprotonated species **7** is ascribed to be originated by PET from the secondary amine to the fluorophore unit. When the lone pair of the amine group engages binding a proton (**8**), the PET process is not plausible anymore. However, in these systems, radical ion species have not been tracked with time-resolved spectroscopies.

To shed some light into these processes, the absorption and emission characteristics and the photodeactivation pathways of **7** and **8** were characterized at different levels of theory (see a discussion of their absorption and emission properties in the SI). The potential energy profiles are schematically presented in Figure 2 and the vertical excitation energies at the ground state and at the relaxed excited state optimized geometries are summarized in Table S2. Vertically, at the Franck−Condon region, the S_1 state is the fluorophore-based $\pi\pi^*$ excitation for both **7** and **8**. According to the computed oscillator strengths, S_1 is responsible of the UV−vis characteristics of **7** and **8** and it is the state that it is populated after photoexcitation. Starting from the Franck−Condon point, relaxation on the S_1 PES leads to a minimum structure, $(\pi\pi^*)_{min}$, in Figure 2, from where fluorescence may occur. This deactivation pathway is conserved in both **7** and **8**. Oppositely to **8**, in the case of **7**, a close-lying dark S_2 state of $n\pi^*$ character (i.e., a CT state) is present at the Franck−Condon region (upper in energy by ca. 0.3 eV according to the ADC(2) calculations). The optimized minimum on the S_2 PES, $(n\pi^*)_{min}$, in Figure 2b, is adiabatically located slightly above the $\pi\pi^*$ minimum (by ca. 0.31 eV according to the ADC(2) calculations) but it is the lowest excited state at its optimized geometry. Therefore, a nonadiabatic pathway likely connects the $\pi\pi^*$ and $n\pi^*$ PESs. In order to further characterize this channel, the conical intersection between the S_2 and S_1 states, $(\pi\pi^*/n\pi^*)_{CI}$, was optimized with the CASSCF method (see details in the SI). The conical intersection optimized geometry is presented in Figure 2b. Starting from the bright S_1 state, this funnel geometry is accessed barrierlessly from the Franck−Condon geometry according to the ADC(2) calculations (or with a very small barrier of ca. 0.06 eV at the CASPT2//CASSCF level), so that ultrafast relaxation to $(n\pi^*)_{min}$ will likely occur. Therefore, in the course of internal conversion after light absorption, competition between the population of the wells of the $n\pi^*$ and $\pi\pi^*$ states will take place in **7**. Indeed, time-correlated single photon counting (TCSPC) fluorescence experiments evidenced competition between two decay channels: a fast and a slow component (τ = 0.15 and τ = 5.02 ns, respectively).[45] Under the experimental conditions, the slow decay is predominant, accounting for ca. 74% of the global decay (thus, the quantum yield of the fastest component is ca. 26%). When adding acid (and thus **8** being predominant), the fast component disappears and longer lifetimes are obtained (τ = 7.05 ns).[45] Theses spectroscopic changes are accompanied by the above-mentioned fluorescence enhancement. Therefore, under these circumstances, the slow component can be indistinguishably assigned to the $\pi\pi^*$ deactivation pathway. The faster component, which is of radiationless nature and has previously been attributed to PET, is likely connected to the $n\pi^*$ deactivation channel.

The analysis of the oscillator strengths at the $n\pi^*$ and $\pi\pi^*$ minima (see f = 0.000 and f = 0.127 for **7** with ADC(2), respectively, in Table S2), reveals that the radiative decay will be favored from $(\pi\pi^*)_{min}$, so that the partial fluorescence quenching can already be understood in qualitative terms, like in compounds **1**−**6**. A deeper evaluation of the fluorescence quantum efficiencies requires the concomitant evaluation of the nonradiative decay rates. Therefore, toward a quantitative prediction of the fluorescence properties of **7** and **8** (both lifetimes and efficiencies), the radiative and the nonradiative decay rates from the involved excited states have been computed from first principles. The prediction of these photophysical properties is still relatively demanding from a computational viewpoint for polyatomic molecules. Furthermore, the direct comparison with the experimental results may become a difficult task, especially in cases of multiply competing deactivation processes. To address the decay rates between two adiabatic electronic states, a thermal vibration correlation function formalism was used.[46] This formalism makes use of a

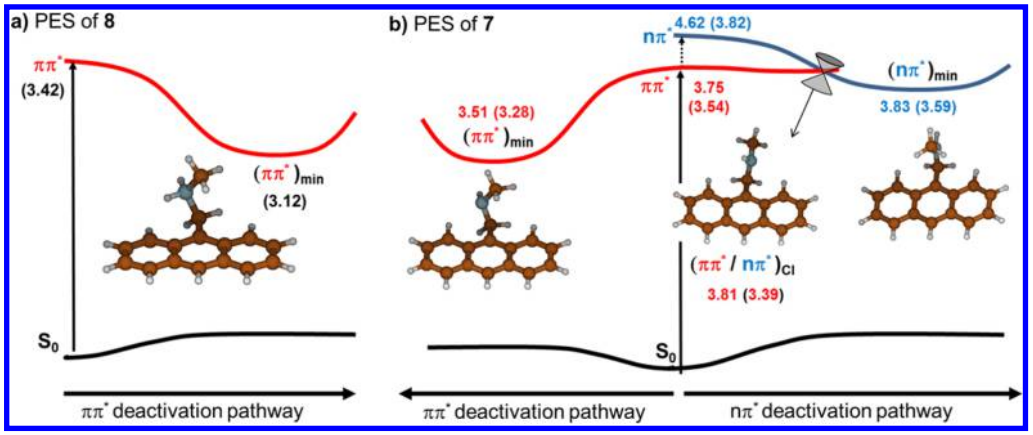

Figure 2. Schematic potential energy profiles for **7** (b) and **8** (a) based on the ADC(2) and CASPT2 calculations (ADC(2) results between parentheses) for the $\pi\pi^*$ and $n\pi^*$ deactivation pathways. Vertical and adiabatic energies are in eV (all of them computed with respect to the S_0 energy at the Franck−Condon point).

DOI: 10.1021/acs.accounts.6b00299
Acc. Chem. Res. 2016, 49, 1816−1824

multidimensional harmonic oscillator model coupled with first principle calculations (for these calculations the less costly yet reliable DFT and TD-DFT methods are used), where distortions, displacements, Duschinsky rotation of the PESs and Herzberg−Teller effects are taken into account (see computational details and the theoretical formalisms for the rate calculations in the SI). This strategy has been proven successful for predicting fluorescence properties of several organic polyatomic systems.[47] The photophysics of **8** can be modeled with a two-level system (see Scheme 5a), while the photophysics of **7** requires at least a three-level system (see Scheme 5b). Note that these models are partially oversimplified, since other possible competing mechanisms, such as, e.g., ISC, are neglected. The results of the rate calculations and of the computed fluorescence lifetimes and efficiencies according to the models presented in Scheme 5 are presented in Table 1. The average time spent in a given excited state is provided by the inverse of the sum of all rates depopulating that state. Hence, according to the models presented in Scheme 5, the fluorescence lifetimes (i.e., the $\pi\pi^*$ state lifetimes) can be expressed as

Scheme 5[a]

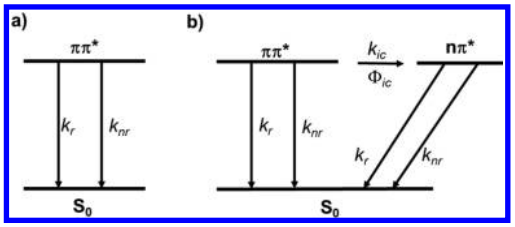

[a](a) Two-state photophysical model for **8**. (b) Three-state photophysical model for **7**.

$$\tau = (k_r + k_{nr})^{-1} \quad (1)$$

where k_r and k_{nr} are the radiative and the nonradiative decay rates from the $\pi\pi^*$ state. The computed radiative and nonradiative decay rates along with the fluorescent lifetimes computed with eq 1 are shown in Table 1. The computed τ values from the $\pi\pi^*$ state (exemplarily 3.9 ns for **7**) are in good agreement with their experimental counterparts (5.02 ns),[45] and thus they further validate the computational protocol to compute the fluorescence lifetimes. The computed τ value for the nπ^* state of **7** is smaller than the experimental one. A likely explanation of this discrepancy could arise from the simplified photophysical models considered herein. Hence, assuming that the nonadiabatic internal conversion via the conical intersection to the nπ^* state is ultrafast (likely occurring in the fs time scale), the experimental fast component could be originated from a subsequent process related to the depopulation of the nπ^* state. One possible process is ISC. Indeed, for **7**, triplet state formation is observed experimentally.[45] The intrinsic fluorescence efficiencies ($\Phi_{intrinsic}$) arising from each excited state are also presented in Table 1. They are computed according to

$$\Phi_{intrinsic} = k_r/(k_r + k_{nr}) \quad (2)$$

In the case of the nπ^* state, as demonstrated by its $\Phi_{intrinsic}$ value, the nonradiative decay is much preferred over the radiative decay. In the case of **8**, since a two-level model is assumed, the $\Phi_{intrinsic}$ value (10.1%) is, without further transformation, the quantum yield of fluorescence (Φ_{fluo}). Contrarily, for **7**, since a three-level model is used, the fluorescence efficiency (Φ_{fluo}) is given by

$$\Phi_{fluo} = \Phi_{IC}\Phi_{intrinsic}(n\pi^*) + (1 - \Phi_{IC})\Phi_{intrinsic}(\pi\pi^*) \quad (3)$$

where Φ_{IC} is the quantum yield of internal conversion from the $\pi\pi^*$ state to the nπ^* state. This branching yield can be obtained from e.g., excited state nonadiabatic dynamic simulations. Alternatively, it can be derived from TCSPC experiments. By using the experimental value of Φ_{IC} = 26% from ref 42, a Φ_{fluo} value of 8.6% is obtained for **7** using eq 3. This value shows a satisfactory agreement with its experimental counterpart (4.7%), despite the assumptions taken in the construction of the photophysical model. Moreover, the observed enhancement of fluorescence upon acidification of the samples is recovered by the calculations. Thus, the computed Φ_{fluo} value increases from 8.6% to 10.1% when going from **7** to **8**, in agreement with the experimental evidence. Summarizing, this computational work reveals that the presence of a nonradiative internal decay involving a dark state is responsible for the partial quenching of fluorescence in **7** (the so-called herein dark-state quenching mechanism). Still, under the present circumstances, and without further compelling experimental proofs, one cannot discard that a real intramolecular PET mechanism competing to radiative and nonradiative decay will still be operative for **7**, or generally for **1**−**6**. Nevertheless, this work demonstrates that the putative PET mechanism is strictly not necessary to rationalize the quenching of fluorescence in these systems

To sum up, two main scenarios may lead to a partial quenching of fluorescence instead of a complete one (provided that no analyte-free probe remains in solution under the experimental conditions): (i) Branching of the initial excited state population between competing deactivation channels (such as, e.g., the nπ^*−$\pi\pi^*$ competing scenario in **7**). In such a case, both excited states should be the lowest excited states at their optimized geometries and the partial quenching effect is mainly determined by the branching yield. (ii) Global relaxation to a mixed LE/ICT state with a non-negligible oscillator strength. In such a case, the fluorescence quenching is often accompanied by a shift in the emission energy. The partial quenching will be determined by the radiative efficiencies at the final state, which can be estimated from first-principles, as herein shown for **7** and **8**. Finally, from a methodological viewpoint it is important to remark that two

Table 1. Radiative and Nonradiative Decay Rates from the $\pi\pi^*$ and nπ^* Excited States of 7 and 8[a]

compd		k_r (s^{-1})	k_{nr} (s^{-1})	τ (ns)	$\Phi_{intrinsic}$ (%)	Φ_{fluo} (%)
7	$\pi\pi^*$	3.00×10^7	2.26×10^8	3.90 (5.02)[b]	11.7	8.6 (4.7)[b]
	nπ^*	4.09×10^7	3.10×10^{11}	0.003 (0.15)[b]	0.0	
8	$\pi\pi^*$	2.85×10^7	2.53×10^8	3.55 (7.05)[b]	10.1	10.1 (−)[c]

[a]Fluorescence lifetimes and quantum yields according to the models presented in Scheme 5 are also included. [b]The values between parentheses correspond to the experimental values obtained in ethanol from ref 45. [c]The experimental value was not determined. For the sake of comparison, the fluorescence quantum yield of **7** in the presence of an acetylation reagent, i.e., $(Boc)_2O$, and hence also leading to an enhancement of fluorescence (like in **8**) is 26.3%.

DOI: 10.1021/acs.accounts.6b00299
Acc. Chem. Res. 2016, 49, 1816−1824

Scheme 6. Distribution of the Number of Studies Found in the Literature during the Period 1990−2016[a]

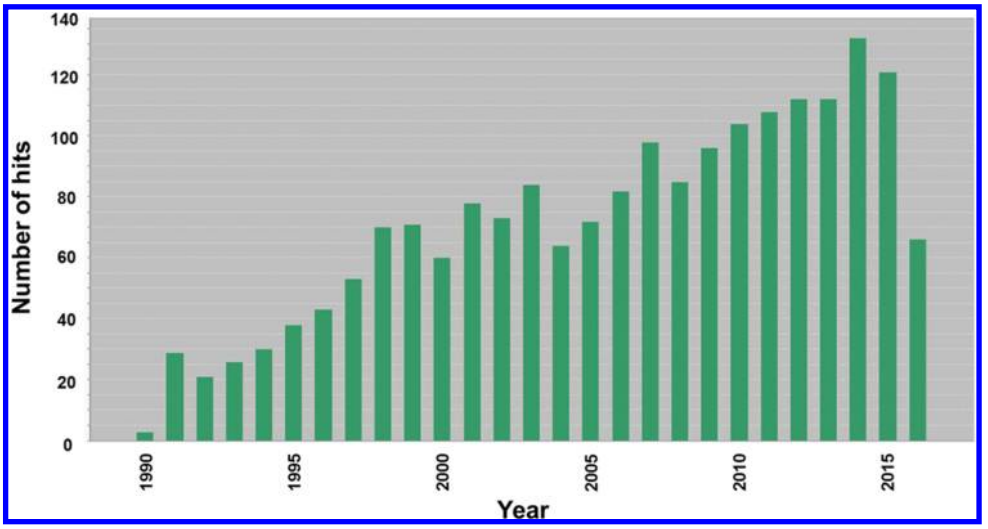

[a]The search parameters were "photoinduced electron transfer" and "fluorescence quenching".

different computational protocols, based on either TD-DFT or CASPT2//CASSCF calculations, have been used to describe the excited state PESs of fluorescent probes. In practical terms it would be interesting to identify beforehand potential data (either of computational or experimental nature) that could alert from the need to use one protocol or the other. The computationally cheaper TD-DFT method is generally recommended for the first exploratory search of the excited state PESs. This strategy has proven successful for **1**-**6**,**8**. If the state ordering changes at relevant regions of the PES (as in **7**), it is an evident sign that state crossings are involved in the photodeactivation pathways. In these situations, multiconfigurational methods are needed to obtain relevant information about the stationary points (i.e., conical intersections and transition states), since it could be the case that these geometries are not energetically accessible, and therefore not significantly populated after photoexcitation. Experimentally, when unusual photophysical properties are observed (e.g., dual photoluminescence, solvent-induced emission switch), it is indicatory of molecules with very intricate photodeactivation pathways. Therefore, the characterization of their excited state PESs may also require the use of multi-configurational methods.[19,32]

4. CONCLUDING REMARKS AND OUTLOOK

In this Account, the origins of the quenching of fluorescence in a wide variety of single molecule fluorescent probes are revisited with a combination of quantum chemical tools. The putative intramolecular PET mechanism is believed, often without compelling experimental proofs, to be responsible of the observed fluorescence quenching occurring in the OFF state of a fluorescent sensor/switch. Quoting Prassana de Silva and co-workers:[48] "Hardly a week goes by without a fluorescent PET sensor being reported." Certainly, this quote from 2009 is still valid in 2016. Indeed, a literature survey of "photoinduced electron transfer" and "fluorescence quenching" provides 1957 hits,[49] see their distribution over the latest 26 years in Scheme 6, and hence stressing the need to put on firmer grounds the fluorescence quenching mechanisms. Herein, through the exploration of the PESs of the lowest-lying excited states and the computation of the radiative and nonradiative efficiencies, it is shown that PET is strictly not necessary to rationalize the quenching of fluorescence in these probes. Instead, enhanced nonradiative deactivation pathways arising from dark states of different nature (the herein called dark-state quenching mechanism), are responsible of this phenomenon. Certainly, further experimental support is needed to prove the existence of PET in these systems. One possible scenario might be when these dark-states are long-lived, so that PET can eventually compete to nonradiative decay to the ground state. For future exploratory searches beyond the common strategy of analyzing frontier molecular orbital energy diagrams, a computational protocol that permits the estimation of the quenching effect in a semiquantitative basis, is proposed. Its success is demonstrated for a wide variety of fluorescent probes, including proton, cation and anion targets. Furthermore, the dark-state quenching mechanism provides a general picture of the fluorescence quenching, that englobes ratiometric quenching, ICT, and those radiationless mechanisms believed to be originated by PET. This mechanism is presumably transferable to other possible scenarios, such as fluorescent probes for transition metal atoms,[50] although for these systems ISC mechanisms are also concomitantly enhanced. Additionally, as demonstrated for **7** and **8**, this study provides for the first time a computational protocol to quantitatively estimate the quenching effect. Finally, from a computational viewpoint it is important to remark that TD-DFT succeds to provide an adiabatic description of the lowest-lying excited states of many fluorescent probes. In the case that surface crossings arise, such as in **7**, multiconfigurational methods are mandatory to describe their deactivation pathways. Future work should be devoted to study the influence of solvent, which importantly modulates the fluorescence properties and thereto the dark-state quenching mechanisms.

■ ASSOCIATED CONTENT

Supporting Information

The Supporting Information is available free of charge on the ACS Publications website at DOI: 10.1021/acs.accounts.6b00299.

Computational details, Cartesian coordinates of the optimized geometries, theoretical formalism for the radiative and nonradiative rates, and summary of the

DOI: 10.1021/acs.accounts.6b00299
Acc. Chem. Res. 2016, 49, 1816−1824

absorption and emission properties of compounds **1**−**8** (PDF)

AUTHOR INFORMATION

Corresponding Author

*E-mail: Daniel.escudero@univ-nantes.fr.

Notes

The author declares no competing financial interest.

Biography

Daniel Escudero was born in Palma de Mallorca (Spain) and received his Ph.D. in Chemistry from the Friedrich-Schiller University (Jena, Germany) in 2011. Following his Ph.D., he moved to the Max-Planck-Institut für Kohlenforschung (Mülheim an der Ruhr, Germany) as a postdoctoral researcher. Since November 2014, he is a postdoctoral researcher at the Université de Nantes (France) and he has recently been awarded an individual Marie-Sklodowska Curie Action. His main research interests are focused on modeling electronically excited states of transition metal complexes and organic compounds.

ACKNOWLEDGMENTS

D.E. acknowledges the European Research Council (ERC) and the Région des Pays de La Loire for his postdoctoral grant (Marches − 278845). Claudiu-Dimitru Sergentu is acknowledged for careful reading of the paper.

REFERENCES

(1) *Electron Transfer in Chemistry*; Balzani, V., Ed.; Wiley-VCH: Weinheim, Germany, 2001.

(2) Natali, M.; Campagna, S.; Scandola, F. Photoinduced Electron Transfer across Molecular Bridges: Electron- and Hole-Transfer Superexchange Pathways. *Chem. Soc. Rev.* **2014**, *43*, 4005−4018.

(3) Grätzel, M. Dye-Sensitized Solar Cells. *J. Photochem. Photobiol., C* **2003**, *4*, 145−153.

(4) Daly, B.; Ling, J.; de Silva, A. P. Current Developments in Fluorescent PET (Photoinduced Electron Transfer) Sensors and Switches. *Chem. Soc. Rev.* **2015**, *44*, 4203−4211.

(5) Stennett, E. M. S.; Ciuba, M. A.; Levitus, M. Photophysical Processes in Single Molecule Organic Fluorescent Probes. *Chem. Soc. Rev.* **2014**, *43*, 1057−1075.

(6) Gray, H. B.; Winkler, J. R. Electron Flow through Metalloproteins. *Biochim. Biophys. Acta, Bioenerg.* **2010**, *1797*, 1563−1572.

(7) Hammarström, L. Accumulative Charge Separation for Solar Fuels Production: Coupling Light-Induced Single Electron Transfer to Multielectron Catalysis. *Acc. Chem. Res.* **2015**, *48*, 840−850.

(8) Marcus, R. A. Electron Transfer Reactions in Chemistry: Theory and Experiment (Nobel Lecture). *Angew. Chem., Int. Ed. Engl.* **1993**, *32*, 1111−1121.

(9) Closs, G. L.; Miller, J. R. Intramolecular Long-Distance Electron Transfer in Organic Molecules. *Science* **1988**, *240*, 440−447.

(10) Weller, A. Photoinduced electron transfer in solution: exciplex and radical ion pair formation free enthalpies and their solvent dependence. *Z. Phys. Chem.* **1982**, *133*, 93−98.

(11) Williams, R. M.; Braslavsky, S. E. Triggering of Photomovement − Molecular Basis. In *Photomovement*; Häder, D.-P., Lebert, M., Eds.; Comprehensive Series in Photosciences; Elsevier Science B.V.: Amsterdam, 2001; Vol. *1*, pp 15−50.

(12) Orzel, L.; Janczyk, A.; Brindell, M.; Stopa, G.; Stochel, G. New Trends in the Application of Laser Flash Photolysis − Case Studies. *J. Coord. Chem.* **2010**, *63*, 2695−2714.

(13) Miura, T.; Urano, Y.; Tanaka, K.; Nagano, T.; Ohkubo, K.; Fukuzumi, S. Rational Design Principle for Modulating Fluorescence Properties of Fluorescein-Based Probes by Photoinduced Electron Transfer. *J. Am. Chem. Soc.* **2003**, *125*, 8666−8671.

(14) Fukuzumi, S.; Ohkubo, K.; Suenobu, T. Long-Lived Charge Separation and Applications in Artificial Photosynthesis. *Acc. Chem. Res.* **2014**, *47*, 1455−1464.

(15) Vlcek, A., Jr.; Kvapilová, H.; Towrie, M.; Zalis, S. Electron-Transfer Acceleration Investigated by Time Resolved Infrared Spectroscopy. *Acc. Chem. Res.* **2015**, *48*, 868−876.

(16) Delor, M.; Scattergood, P. A.; Sazanovich, I. V.; Parker, A. W.; Greetham, G. M.; Meijer, A. J. H. M.; Towrie, M.; Weinstein, J. A. Toward Control of Electron Transfer in Donor-Acceptor Molecules by Bond-Specific Infrarred Excitation. *Science* **2014**, *346*, 1492−1495.

(17) Batat, P.; Vives, G.; Bofinger, R.; Chang, R.-W.; Kauffmann, B.; Oda, R.; Jonusauskas, G.; McClenaghan, N. D. Dynamics of Ion-Regulated Photoinduced Electron Transfer in BODIPY-BAPTA Conjugates. *Photochem. Photobiol. Sci.* **2012**, *11*, 1666−1674.

(18) Su, H.; Chen, X.; Fang, W. ON-OFF Mechanism of a Fluorescent Sensor for the Detection of Zn(II), Cd(II), and Cu(II) Transition Metal Ions. *Anal. Chem.* **2014**, *86*, 891−899.

(19) Pérez-Ruiz, R.; Griesbeck, A. G.; Sampedro, D. Computational Study on Fluoride Recognition by an Urea-Activated Pthalimide Chemosensor. *Tetrahedron* **2012**, *68*, 5724−5729.

(20) Niu, Y.; Peng, Q.; Deng, C.; Gao, X.; Shuai, Z. Theory of Excited State Decays and Optical Spectra: Application to Polyatomic Molecules. *J. Phys. Chem. A* **2010**, *114*, 7817−7831.

(21) Escudero, D.; Jacquemin, D. Computational Insights into the Photodeactivation Dynamics of Phosphors for OLEDs: a Perspective. *Dalton Trans.* **2015**, *44*, 8346−8355.

(22) Escudero, D. Quantitative Prediction of Photoluminescence Quantum Yields from First Principles. *Chem. Sci.* **2016**, *7*, 1262−1267.

(23) Orlandi, G.; Zerbetto, F.; Zgierski, M. Z. Theoretical Analysis of Spectra of Short Polyenes. *Chem. Rev.* **1991**, *91*, 867−891.

(24) Zgierski, M. Z.; Fujiwara, T.; Lim, E. C. Role of the $\pi\sigma^*$ State in Molecular Photophysics. *Acc. Chem. Res.* **2010**, *43*, 506−517.

(25) Polívka, T.; Sundström, V. Ultrafast Dynamics of Carotenoid Excited-States − From Solution to Natural and Artificial Systems. *Chem. Rev.* **2004**, *104*, 2021−2071.

(26) Qi, J.; Liu, D.; Liu, X.; Guan, S.; Shi, F.; Chang, H.; He, H.; Yang, G. Fluorescent pH Sensors for Broad-Range pH Measurement Based on a Single Fluorophore. *Anal. Chem.* **2015**, *87*, 5897−5904.

(27) Walker, A. S.; Rablen, P. R.; Schepartz, A. Rotamer-Restricted Fluorogenicity of the Bis-Arsenical ReAsH. *J. Am. Chem. Soc.* **2016**, *138*, 7143−7150.

(28) Christianson, A. M.; Gabbaï, F. P. Synthesis and Coordinationn Chemistry of a Phosphine-Decorated Fluorescein: "Double Turn-On" Sensing of Gold(III) Ions in Water. *Inorg. Chem.* **2016**, *55*, 5828.

(29) Hutt, J. T.; Jo, J.; Olasz, A.; Chen, C.-H.; Lee, D.; Aron, Z. D. Fluorescence Switching of Imidazo[1,5-a]pyridinium Ions: pH-Sensors with Dual Emission Pathways. *Org. Lett.* **2012**, *14*, 3162−3165.

(30) Oshima, J.; Shiobara, S.; Naoumi, H.; Kaneko, S.; Yoshihara, T.; Mishra, A. K.; Tobita, S. Extreme Fluorescence Sensitivity of Some Aniline Derivatives to Aqueous and Nonaqueous Environments: Mechanistic Study and Its Implication as Fluorescence Probe. *J. Phys. Chem. A* **2006**, *110*, 4629−4637.

(31) Park, M.; Kim, C. H.; Joo, T. Multifaceted Ultrafast Intramolecular Charge Transfer Dynamics of 4-(Dimethylamino)-benzonitrile (DMABN). *J. Phys. Chem. A* **2013**, *117*, 370−377.

(32) Segado, M.; Benassi, E.; Barone, V. A "Twist" on the Interpretation of the Multifluorescence Patterns of DASPMI. *J. Chem. Theory Comput.* **2015**, *11*, 4803−4813.

(33) Gómez, I.; Castro, P. J.; Reguero, M. Insight into the Mechanisms of Luminescence of Aminobenzonitrile and Dimethylaminobenzonitrile in Polar Solvents. An ab Initio Study. *J. Phys. Chem. A* **2015**, *119*, 1983−1995.

(34) Coto, P. B.; Serrano-Andrés, L.; Gustavsson, T.; Fujiwara, T.; Lim, E. C. Intramolecular Charge Transfer and Dual Fluorescence of 4-(Dimethylamino)benzonitrile: Ultrafast Branching followed by a Two-Fold Decay Mechanism. *Phys. Chem. Chem. Phys.* **2011**, *13*, 15182−15188.

(35) Grabowski, Z. R.; Rotkiewicz, K.; Rettig, W. Structural Changes Accompanying Intramolecular Electron Transfer: Focus on Twisted

DOI: 10.1021/acs.accounts.6b00299
Acc. Chem. Res. 2016, 49, 1816−1824

Intramolecular Charge-Transfer States and Structures. *Chem. Rev.* **2003**, *103*, 3899−4031.
(36) Segado, M.; Mercier, Y.; Gómez, I.; Reguero, M. Intramolecular Charge Transfer in Aminobenzonitriles and Tetrafluoro Counterparts: Fluorescence Explained by Competition between Low-lying Excited States and Radiationless Deactivation. Part II: Influence of Substitution on Luminescence Patterns. *Phys. Chem. Chem. Phys.* **2016**, *18*, 6875−6884.
(37) Dubey, R. K.; Knorr, G.; Westerveld, N.; Jager, W. F. Fluorescent PET Probes Based on Perylene-3,4,9,10-tetracarboxylic Tetraesters. *Org. Biomol. Chem.* **2016**, *14*, 1564−1568.
(38) Pan, Z.-H.; Luo, G.-G.; Zhou, J.-W.; Xia, J.-X.; Fang, K.; Wu, R.-B. A Simple BODIPY-aniline-based Fluorescent Chemosensor as Multiple Logic Operations for the Detection of pH and CO_2 gas. *Dalton Trans.* **2014**, *43*, 8499−8507.
(39) de Silva, A. P.; de Silva, S. A. Fluorescent Signaling Crown Ethers; "Switching On" of Fluorescence by Alkali Metal Ion Recognition and Binding in situ. *J. Chem. Soc., Chem. Commun.* **1986**, 1709−1710.
(40) Madhu, S.; Ravikanth, M. Boron-Dipyrromethene Based Reversible and Reusable Selective Chemosensor for Fluoride Detection. *Inorg. Chem.* **2014**, *53*, 1646−1653.
(41) Ji, S.; Yang, J.; Yang, Q.; Liu, S.; Chen, M.; Zhao, J. Tuning the Intramolecular Charge Transfer of Alkynylpyrenes: Effect on Photophysical Properties and Its Application in Design of OFF-ON Fluorescent Thiol Probes. *J. Org. Chem.* **2009**, *74*, 4855−4865.
(42) Guo, H.; Jing, Y.; Yuan, X.; Ji, S.; Zhao, J.; Li, X.; Kan, Y. Highly Selective Fluorescent OFF-ON Thiol Probes Based on Dyads of BODIPY and Potent Intramolecular Electron Sink 2,4-Dinitrobenzenesulfonyl Subunits. *Org. Biomol. Chem.* **2011**, *9*, 3844−3853.
(43) Savarese, M.; Raucci, U.; Adamo, C.; Netti, P. A.; Ciofini, I.; Rega, N. Non-radiative Decay Paths in Rhodamines: New Theoretical Insights. *Phys. Chem. Chem. Phys.* **2014**, *16*, 20681−20688.
(44) Dondaine, L.; Escudero, D.; Ali, M.; Richard, P.; Denat, F.; Bettaieb, A.; Le Gendre, P.; Paul, C.; Jacquemin, D.; Goze, C.; Bodio, E. Coumarin-Phosphine-Based Smart Probes for Tracking Biologically Relevant Metal Complexes: From Theoretical to Biological Investigations. *Eur. J. Inorg. Chem.* **2016**, *2016*, 545−553.
(45) Xu, K.; Zhao, J.; Escudero, D.; Mahmood, Z.; Jacquemin, D. Controlling Triplet-Triplet Annihilation Upconversion by Tuning the PET in Aminomethyleneanthracenes Derivatives. *J. Phys. Chem. C* **2015**, *119*, 23801−23812.
(46) Peng, Q.; Niu, Y.; Deng, C.; Shuai, Z. Vibration Correlation Function Formalism of Radiative and Non-Radiative Rates for Complex Molecules. *Chem. Phys.* **2010**, *370*, 215−222.
(47) Shuai, Z.; Wang, D.; Peng, Q.; Geng, H. Computational Evaluation of Optoelectronic Properties for Organic/Carbon Materials. *Acc. Chem. Res.* **2014**, *47*, 3301−3309.
(48) de Silva, A. P.; Moody, T. S.; Wright, G. D. Fluorescent PET (Photoinduced Electron Transfer) Sensors as Potent Analytical Tools. *Analyst* **2009**, *134*, 2385−2393.
(49) Web of Science, Thomson Reuters, 2016.
(50) Rurack, K. Flipping the Light Switch "ON" − the Design of Sensor Molecules that Show Cation-induced Fluorescence Enhancement with Heavy and Transition Metal Ions. *Spectrochim. Acta, Part A* **2001**, *57*, 2161−2195.

DOI: 10.1021/acs.accounts.6b00299
Acc. Chem. Res. 2016, 49, 1816−1824